Experimental testing and analysis of the axial behaviour of intermeshed steel connections

McGetrick, Patrick J.; Robinson, Desmond; Matis, Pantelis; Martin, Tony; Laefer, Debra F.; Al-Sabah, Salam; Truong-Hong, Linh; Huynh, Minh Phuoc; Schultz, Arturo E.; Le, Jia Liang

DOI
10.1680/jstbu.19.00181

Publication date
2021

Document Version
Final published version

Published in
Proceedings of the Institution of Civil Engineers: Structures and Buildings

Cite this article
McGetrick PJ, Robinson D, Matis P *et al.*
Experimental testing and analysis of the axial behaviour of intermeshed steel connections.
Proceedings of the Institution of Civil Engineers – Structures and Buildings,
https://doi.org/10.1680/jstbu.19.00181

Research Article
Paper 1900181
Received 09/09/2019;
Accepted 05/10/2020

Keywords: buildings, structures & design/recycling & reuse of materials/ steel structures

Structures and Buildings

ice Publishing

Experimental testing and analysis of the axial behaviour of intermeshed steel connections

Patrick J. McGetrick BEng, PhD
Lecturer, School of Engineering, National University of Ireland, Galway, Ireland; School of Natural and Built Environment, Queen's University Belfast, Belfast, Northern Ireland (Orcid:0000-0001-5373-2334) (corresponding author: patrick.mcgetrick@nuigalway.ie)

Desmond Robinson PhD
Senior Lecturer, School of Natural and Built Environment, Queen's University Belfast, Belfast, Northern Ireland

Pantelis Matis BEng, MSc
Doctoral Candidate, School of Natural and Built Environment, Queen's University Belfast, Belfast, Northern Ireland

Tony Martin BEng(Hons), MSc, DIC, PhD, CEng, MIStructE
Lecturer, School of Natural and Built Environment, Queen's University Belfast, Belfast, Northern Ireland

Debra F. Laefer PhD
Professor, Center for Urban Science and Progress and Department of Civil and Urban Engineering, Tandon School of Engineering, New York University, New York, NY, USA; School of Civil Engineering, University College Dublin, Dublin, Ireland (Orcid:0000-0001-5134-5322)

Salam Al-Sabah PhD, CEng
Research Fellow, School of Civil Engineering, University College Dublin, Dublin, Ireland (Orcid:0000-0002-9856-4159)

Linh Truong-Hong BEng, MEng, PhD, MIEI
Researcher, Department of Geoscience & Remote Sensing, TU Delft, the Netherlands (Orcid:0000-0003-2126-6409)

Minh Phuoc Huynh PhD, MIEI
Research Fellow, School of Civil Engineering, University College Dublin, Dublin, Ireland (Orcid:0000-0002-9486-4330)

Arturo E. Schultz PhD, fPCI, fTMS
Professor and Chair, Department of Civil and Environmental Engineering, The University of Texas at San Antonio, San Antonio, TX, USA; Professor Emeritus, Department of Civil, Environmental and Geo-Engineering, University of Minnesota, Minneapolis, MN, USA (Orcid:0000-0001-5311-8000)

Jia-Liang Le BEng(Hons), MEng, PhD, PE
Associate Professor, Department of Civil, Environmental and Geo-Engineering, University of Minnesota, Twin Cities, Minneapolis, MN, USA (Orcid:0000-0002-9494-666X)

Mohammad E. Shemshadian PhD
Doctoral Candidate, Graduate Research Assistant, Department of Civil, Environmental and Geo-Engineering, University of Minnesota, Twin Cities, Minneapolis, MN, USA (Orcid:0000-0003-2210-9691)

Ramzi Labbane MS
Research Assistant, Department of Civil, Environmental and Geo-Engineering, University of Minnesota, Twin Cities, Minneapolis, MN, USA

This paper presents the work carried out on a collaborative tripartite project between the USA, Republic of Ireland and Northern Ireland to create and investigate the design, development and testing of a new class of intermeshed steel connections (ISCs) that do not rely on field welding and minimise bolting, thus targeting the facilitation of fast disassembly of steel structures and material reuse. This research took advantage of fully automated, precise, advanced manufacturing cutting technologies (e.g. laser, waterjet and high-definition plasma cutting) to achieve a connection method in steel that previously was only possible in materials such as timber, with the potential to revolutionise the steel construction industry. The paper outlines the ongoing research work by the collaborative team, focusing on the design, fabrication, finite-element analysis (FEA) and scaled experimental testing of side ISCs for the flanges of open sections, which included the use of state-of-the-art digital image correlation technology for non-contact measurements. A simplified connection design procedure is presented based on yielding of the side plates. This design procedure is refined based on the results of experimental testing and FEA of the local axial behaviour of the flange connection, addressing stress concentrations in the flange, fabrication tolerances and material overstrength.

Notation

A_f	flange effective area
A_{sp}	side plate net effective area provided
$A_{sp,req}$	side plate required effective area
$A_{v,tooth}$	tooth shear area
b_t	flange tooth width
E	Young's modulus
F_t	total force in flange
F_{ti}	force per flange side
$F_{y,sp,max}$	maximum potential yield resistance of side plate
$F_{y,sp,min}$	minimum yield resistance of side plate
f_u	material ultimate tensile strength
f_y	material yield strength
f_{yr}	reduced material yield strength for shear area
g_0	tolerance between side plate and flange
l_{sp}	side plate length
l_t	flange tooth length
M_{Ed}	tooth design bending moment
$M_{pl,Rd}$	tooth plastic moment resistance
$M_{pl,V,Rd}$	reduced tooth plastic moment resistance
n_t	number of teeth per flange side
$n_{t,rev}$	revised number of teeth per flange side
r_t	flange tooth corner radius
t_f	flange thickness
t_{sp}	side plate thickness
V_{Ed}	design shear force in tooth
$V_{pl,Rd}$	plastic shear resistance of each flange tooth
$W_{pl,z,tooth}$	tooth plastic section modulus
γ_{M0}	partial safety factor for resistance of cross-section
ν	Poisson's ratio
ρ	factor for bending stress reduction
τ_y	shear yield strength

1. Introduction

A new, universally applicable, structural steel connection mechanism has not been introduced in more than a century. Bolting and welding remain the two primary options for connecting structural steel elements on site, despite both being expensive and time-consuming operations. In addition, with these connection options, easy disassembly cannot always be facilitated for material reuse (BCSA *et al.*, 2018a; Sansom and Avery, 2014), particularly in the case of welding. It is notable that this remains the case even though steel is the most recycled construction material (SRI, 2017).

However, recent advances in manufacturing technologies have created a platform that enables the development of a new universal connection in steel. To date, advanced cutting technologies have only been used to accelerate traditional processes by cutting sheet metal or providing faster conventional fabrication (e.g. cutting instead of drilling bolt holes). This paper presents an overview of a collaborative tripartite research project, entitled Advanced manufacturing and assembly of steel structures (AMASS), which is the first of its kind to exploit fully automated, precise, advanced manufacturing cutting technologies (e.g. laser, waterjet and high-definition (HD) plasma cutting) in the creation of a new class of efficient intermeshed steel connections (ISCs) (Al-Sabah and Laefer, 2017a, 2017b; Al-Sabah *et al.*, 2020) that eliminate the need for on-site welding and most on-site bolting.

The potential impact of an alternative steel connection of this type that targets reductions in time and cost and simplifies disassembly for reuse is further highlighted by the dominance of steel in the construction industry. Considering the UK alone, structural steelwork currently holds a dominant share of 67% in the multi-storey buildings market and similar shares (~60%) are reflected in corresponding EU markets (Muller, 2008). In the USA, the structural steel market size for both residential and non-residential construction has grown steadily since 2014 (GVR, 2019). For a typical multi-storey commercial building, fabrication costs can rival the material costs, reaching 30–40% of the overall cost (BCSA *et al.*, 2018b). Furthermore, a major part of the steel frame cost (10–15%) is related to on-site assembly and erection, with longer schedules and higher associated costs expected for more complex connections. The AMASS project aims to deliver an efficient new connection that improves and refines these features of steel buildings and structures, including bridges, leading to savings in time and hence cost across the UK and EU construction industries, in addition to fast-growing markets in the USA, China and India.

Recent decades have seen the proposal of alternatives to existing steel connections, a number of which were motivated by the brittle failure mechanism of steel moment-resisting connections during the 1994 Northridge earthquake (AISC, 2016a; FEMA, 2000; Hamburger *et al.*, 2009; Han and Moon, 2007; Naimi *et al.*, 2013; SAC JV, 1995; Stojadinovic *et al.*, 2000). While proprietary connection solutions have resulted, these have limited use in wider practice and thus have had limited success (Cordova and Hamburger, 2011). Among the most successful alternative connections developed in the USA are the Kaiser bolted bracket moment connection (Adan and Gibb, 2008, 2009), the ConXL moment connection (ConXtech, 2020; Hamburger, 2006), the ATLSS connection (Fleischman *et al.*, 1990; Perreira *et al.*, 1993), the SidePlate connection (Rafezy *et al.*, 2015, 2018), the reduced beam section moment connection (Engelhardt *et al.*, 1998; Jin and El-Tawil, 2005) and the pin–fuse connection (Cordova and Hamburger, 2011). Alternative connections have also been developed in the UK, such as the Lindsay adapter (Lindapter, 2018) and the Quicon connection (Burgan, 2002; Heywood, 2004), designed by the UK Steel Construction Institute. However, all the above continue to rely predominantly on conventional bolted or welded methods or require more expensive casting techniques.

The ISC method developed by the AMASS project team eliminates the need for these on-site operations by means of a 'snap together' connection mechanism. This mechanism is summarised in Section 2 for two types of ISC – the front ISC and the side ISC. Section 3 details the fabrication, design and scaled experimental testing of the flange connection component of the side ISC, with a focus on its axial behaviour. Section 4 presents the results of finite-element analysis (FEA) of the tested connections while Section 5 provides a brief design review and recommendations for future design.

2. ISC method

The ISC method employs advanced manufacturing technologies to create precise geometries that snap together, with load transfer achieved through common bearing surfaces at multiple contact points. The fabrication of such geometries from both two- and three-dimensional steel sections is now possible due to the introduction of computer numerical control technology and robotic arms in conjunction with advanced cutting technologies such as laser, waterjet and HD plasma cutting and wire electrical discharge machining (WEDM) (Krar and Gill, 2003; Ramakrishnan and Rogozinski, 1997). A comparison of these cutting technologies is provided in Table 1. For the experimental work described in this paper, the typical cutting tolerance achieved for connection samples was ± 0.2 mm using a flatbed laser cutter.

2.1 Front ISC

Figure 1 shows the first type of ISC developed – the front ISC (Al-Sabah and Laefer, 2017a). Bending moment is transferred across the connection by way of tension and compression in the two flanges; this is achieved by bearing and friction by the intermeshed 'teeth' of the flanges, the dovetail configuration of which can also be seen in Figure 1. Shear load transfer is achieved by direct contact bearing at multiple points along the

Table 1. General comparison of metal cutting technologies

	Waterjet cutting	Plasma cutting	Laser cutting	WEDM
Cutting method	Erosion	Melt and blow	Melt and blow	Electric spark erosion
Maximum thickness: mm	300	60	20	300
Speed	2–12 mm/s	4–600 mm/s	1.5–300 mm/s	150–500 mm^2/s
Tolerance (for 10 mm thickness): mm	±0.05–0.2	±0.25–0.4	±0.025–0.08	0.005
Bevel angle: degree	1	Up to 5	1	None
Equipment cost US$	60 000–300 000	60 000–300 000	400 000–1 000 000	25 000–100 000
Cut finish	Good–excellent	Good	Good–excellent	Excellent
Kerf thickness: mm	0.5–1.3	1.5–2	0.7–1.5	0.021–0.41
Dross	None	Small, can be controlled	Small, can be controlled	None
Heat-affected zone	None	Large	Better than plasma	Small

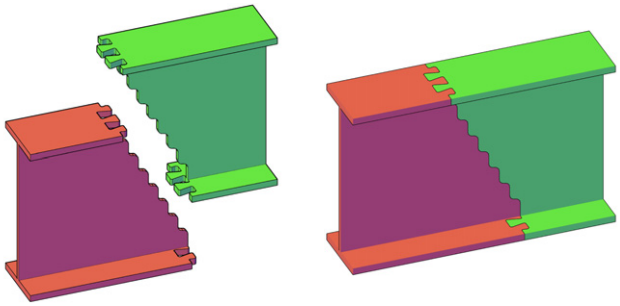

(a) (b)

Figure 1. Front ISC: (a) prior to assembly; (b) fully assembled

stepped web connection, while a small locking piece can be inserted to provide resistance to uplift or unexpected lateral loading. The arrangement is ideally suited for connecting beams at or near-ideal inflection points to create gravity load framing, as illustrated in Figure 2, where beam stubs can be welded to columns off-site. The connection geometry also lends itself to a straightforward assembly and disassembly on site, which is desirable – a beam can be dropped into place prior to inserting the locking element. However, it is worth noting that this also means the connection is primarily suited to scenarios where cutting and site erection tolerances are expected to be small and highly controlled. Furthermore, as a new connection type with faying surfaces, careful attention needs to be paid to the type of coating system used if a spray or paint is to be applied for fire or corrosion protection (NSAI, 2018). As the front ISC relies on bearing and friction for load transfer, it is preferable that any applied coating provides a specified slip factor (friction coefficient) of at least a value of 0.3 for the surfaces in contact, verified by testing in accordance with the relevant standard (BSI, 2011). In the case of possible damage to the coating, the connection can be inspected after installation and any damage to the paint repaired as necessary.

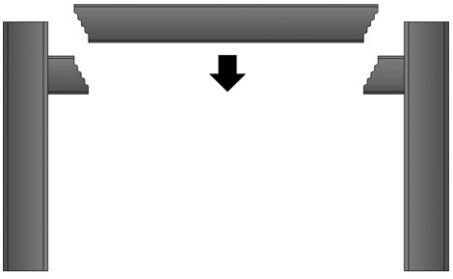

Figure 2. Beam erection mechanism for gravity load framing using front ISC

2.1.1 Summary of the behaviour of the front ISC under mixed-mode loading

The related load-transfer behaviour and performance of the front ISC connection type have already been studied numerically under simulated mixed-mode loading scenarios by the authors (Shemshadian *et al.*, 2019) for a 254×102 UB 28 beam section, with the connection exhibiting excellent shear resistance even in the presence of flexural and axial loading. The non-linear FEA carried out by the authors enabled the interaction diagrams of axial, shear and moment capacities of this ISC to be obtained; interaction diagrams currently available in design codes were found to be inadequate in capturing the behaviour of the connection.

However, as mentioned earlier, this connection type is sensitive to assembly tolerance and it was found that its axial and flexural behaviour were significantly affected by the alignment of the flanges, which can be altered in response to loading, even for 'perfect' initial configurations, and this alignment can also potentially differ between fabrication and erection due to thermal effects, particularly for long members. Therefore, while it was established that the connection can be classified as a simple, partially restrained (or semi-rigid) connection according to ANSI/AISC 360-16 (AISC, 2016b) and BS EN 1993-1-8:2005 (BSI, 2005) and thus used for gravity load bearing structures, further study of the alignment of the flanges is required in order to better understand how to avoid axial and/or flexural failures. A final recommendation on modelling of this connection is provided, suggesting that the intermeshed connection can be represented as a pin connection, but

limited additional flexural stiffness may be required for a fully accurate numerical representation. The authors have proposed alternative flange geometries in order to improve the axial and flexural capacities of this connection type and work in this area is ongoing (Matis *et al.*, 2018a, 2018b).

2.2 Side ISC

Figure 3 shows the second type of ISC developed – the side ISC (Al-Sabah and Laefer, 2017b). This connection is an improvement on the front ISC configuration and can accommodate greater tolerances in assembly and fabrication through the introduction of side plates at the top and bottom flanges, which transfer tension and compression forces resulting from bending moments. For this purpose, teeth are cut along the flange edges, which allow side plates with matching holes to be slotted into position. The side plates can then be fixed in place using a variety of methods, including T-head bolts (configuration shown in the figure). As per the front ISC, shear load transfer can also be achieved by direct contact bearing at multiple points along the stepped web connection, as shown in Figure 1. However, an alternative version is illustrated in Figure 3, which targets greater acceptance in the construction industry using bolted shear web plates to achieve shear load transfer. The configuration shown in Figure 3 is for a 254×146 UB 31 beam section; the dimensions of the four side plates are $557 \times 65 \times 10$ mm while those of the two web plates are $200 \times 201 \times 5$ mm. Slots are provided in the flange teeth to allow eight T-head M8 grade 8.8 bolts to fix the side plates in place while eight M12 grade 8.8 bolts are used for the web plate (not shown). Due to the predominance of flatbed cutting machines used in industry at present, the fabrication of built-up sections to form the side ISC is also possible, offering potential applications for longer span beams and bridge structures.

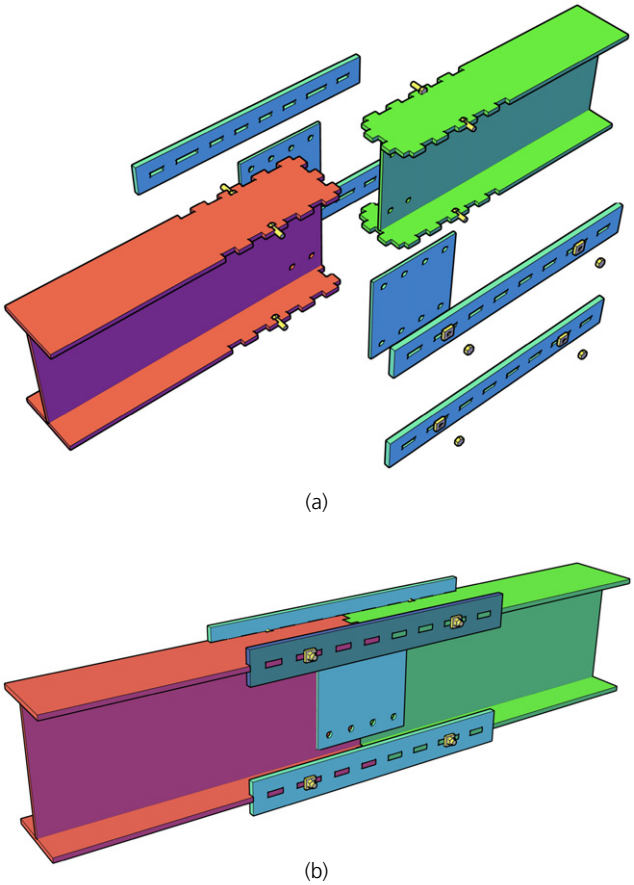

Figure 3. Side ISC: (a) prior to assembly; (b) fully assembled

The behaviour and performance of this connection type are currently under ongoing investigations by the AMASS team. The experimental testing and FEA of scaled flange connections under tensile loading are presented in Sections 3 and 4 of this paper respectively, investigating the local axial behaviour of the side ISC in flanges and side plates. A description of the full-scale beam testing programme is outside the scope of this paper, but the authors have recently reported the results of an experimental testing programme (Shemshadian *et al.*, 2020) in which simply-supported beams utilising the side ISC with side angles were designed to resist gravity loading in frames, and were tested under pure bending and combined bending and shear. In all cases, the beam connections performed as intended but were found to provide a greater moment capacity than designed for; this was attributed to material overstrength and a conservative design procedure. These factors are also addressed in this paper regarding the axial performance of the scaled connection with side plates.

2.2.1 Side ISC constructability and erection time

To investigate the constructability and erection time requirements of the side ISC, a trial erection test of the connection in a two-storey assembly has been completed recently (Al-Sabah *et al.*, 2020) and a video report on this can be viewed online (UMG, 2019). The trial assembly included geometric deviations in connection fabrication within the tolerances accepted by the steel industry. It also included the use of shim plates to introduce the maximum allowable site tolerances in the column (10 mm shim under the base plate) and beam stub (1 mm shims) alignments for erection. It is notable that these deviations did not cause any delay in the frame erection. As a primary cost benefit for this connection type relates to the efficiency of assembly and disassembly, this was also analysed during the trial erection test. It was found that the side ISC assembly provided a fast learning curve, with completion time decreasing from 12 min 58 s initially per beam connection to an average completion time of 4 min 32 s for the last two connections. Subsequent disassembly was also straightforward and much faster, averaging around 2 min 30 s per beam connection.

The average web splice plate installation time was 2 min 27 s. This involved installing the two plates, inserting and tightening

eight M12 bolts, giving an average time per individual M12 bolt of around 18 s. It is expected that this time would increase with bolt diameter. For the equivalent bolted beam splice connection, 40 M12 bolts would be required, with ten on each side of the two splice plates for the flanges. The time required to assemble this connection, based on the average 18 s per bolt in the frame test, would be 18 s × 40 bolts = 720 s = 12 min. Note that these times ignore the fitting time for the heavier flange splice plate as it should not add much to the total time. Based on these average assembly times, the ISC could potentially offer a time saving of 62.5% over conventional bolted connections – which is significant. Further work is required to establish definitively the fabrication costs and erection times relative to equivalent bolted and welded connections, including on-site erections. To this end, an equivalent bolted frame assembly test is planned.

3. Experimental study of the axial behaviour of the side ISC

This section presents the results of uniaxial testing of scaled flange geometries for the side ISC. Due to the potential issues encountered with the misalignment of beam flanges for the front ISC, it is important to study the axial behaviour of this connection type experimentally to verify the design procedure and identify any factors that could potentially influence its behaviour at full scale.

3.1 Experimental test setup

Tensile tests were carried out with a displacement rate of 1 mm/min using a Zwick/Roell RetroLine tC II universal testing machine (UTM) (Figure 4(a)), which was calibrated in accordance with ISO 7500-1 (BSI, 2004a). This had a tensile capacity of 100 kN with an accuracy of ± 2% and cross-head speed range of 0.001–1000 mm/min. Tinius Olsen mechanical wedge action grips were used to hold samples in place.

Load measurements were directly output by the UTM control system, while sample deformations were measured using a LaVision StrainMaster portable digital image correlation (DIC) system (LaVision, 2018) (Figure 4(b)). DIC is a non-invasive technique that can be used to measure deformations by analysing a series of images (Sutton *et al.*, 2009) and, in these tests, allowed deformations to be observed across full samples rather than at one localised strain gauge location. For this purpose, test samples were spray painted with a matt black and white speckle pattern that the DIC system could track and analyse. The system comprised a dedicated laptop computer running LaVision StrainMaster analysis software along with the following components mounted on an adjustable lightweight bar and tripod, as shown in Figure 4(b)

- 2 × VC-Imager E-lite cameras (5 megapixels, USB3)
- a compact controller unit
- 2 × 20 W LED linear illumination units producing focused white light.

3.1.1 Sample connection geometry

The scaled flange geometry tested in this study is shown in Figure 5; this geometry ensured that connection behaviour up to failure could be observed; that is, the failure load would not exceed the capacity of the UTM (100 kN). In total, six samples of this arrangement were laser cut from 6 mm S275JR

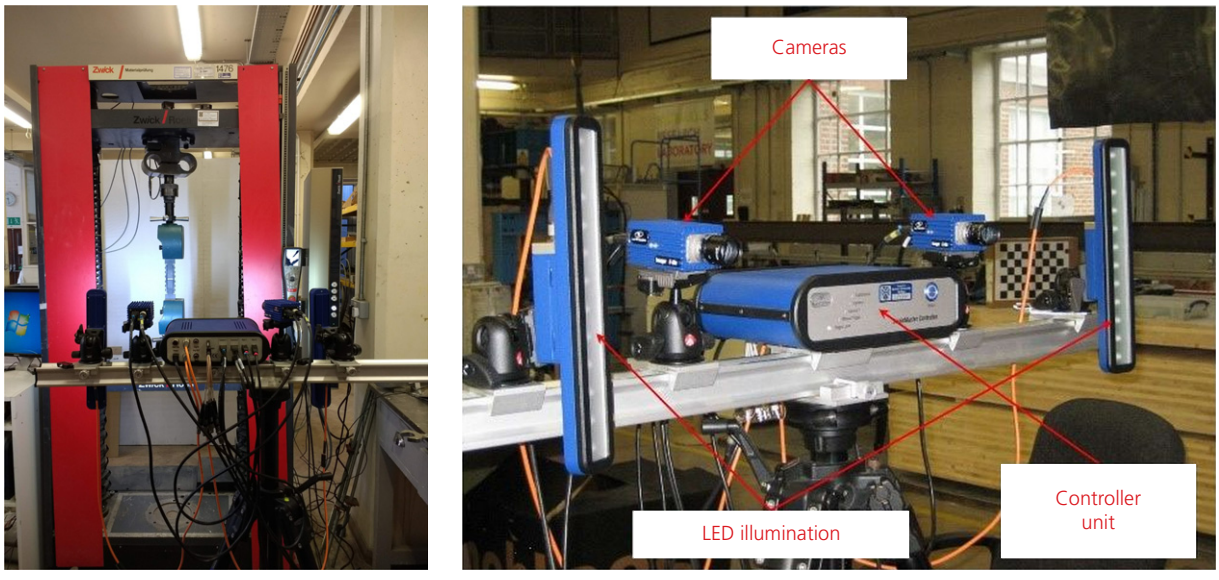

Figure 4. Experimental test setup: (a) UTM; (b) LaVision StrainMaster portable DIC system

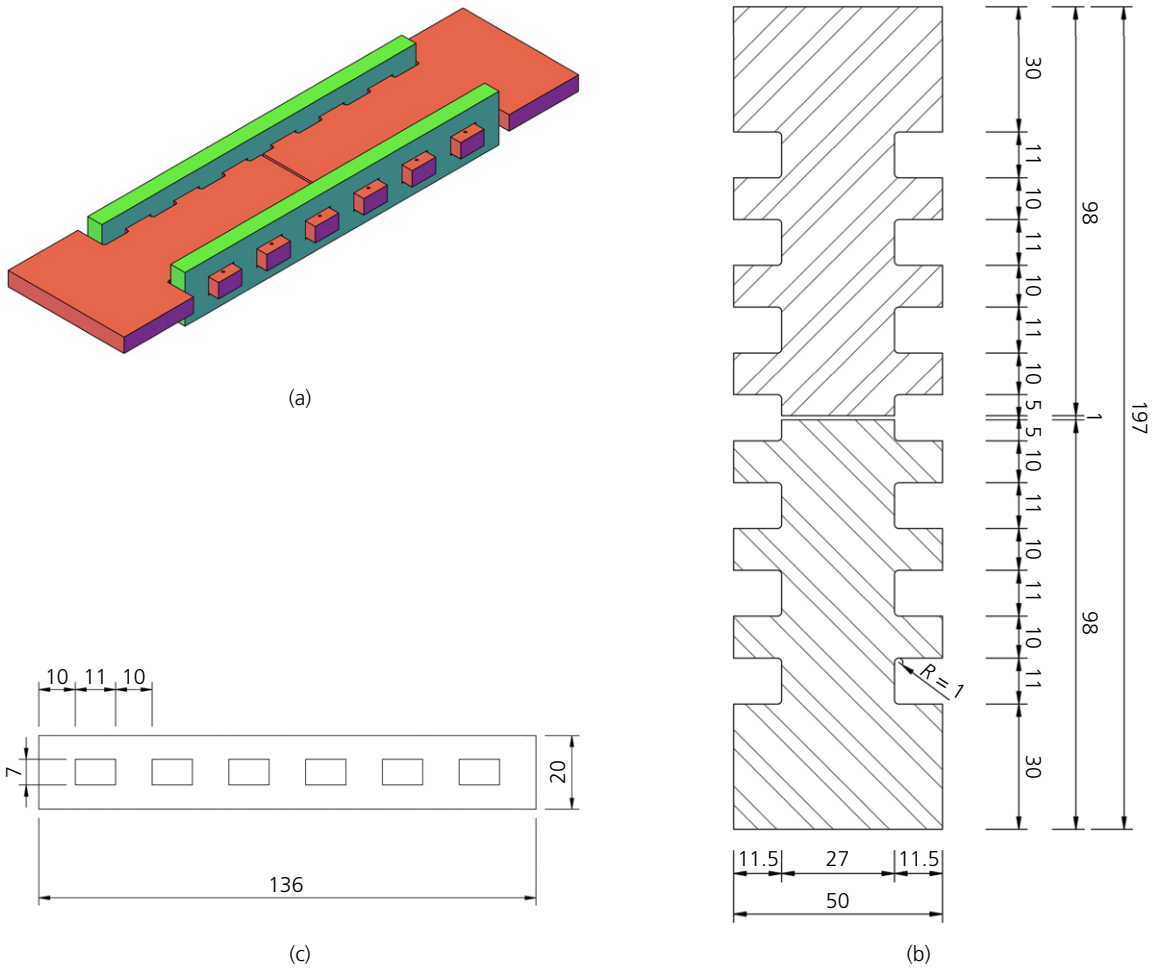

Figure 5. Geometry of scaled side ISC for testing: (a) assembled; (b) flange dimensions; (c) side plate dimensions (all units in mm)

steel plate; thus all components – flanges and side plates – were 6 mm thick. An example of the fabricated geometry is shown in Figure 6(a). Laser cutting is suitable for material thicknesses up to 20 mm. Sample fabrication using a flatbed laser cutter (a Trumpf TruLaser 4050 laser cutting machine) was thus appropriate, with a minimum geometric tolerance of ±0.2 mm specified by the fabricator. As can be seen in Figure 5, the connection design has an allowable tolerance of 1 mm for each slotted hole – that is 10 mm wide × 6 mm thick teeth in 11 mm × 7 mm holes.

In the full-scale connection (Figure 3), M8 bolts are used to hold the side plates in place. However, as the testing scale did not allow for these to be included, for safety purposes during testing, the flange teeth were extended by 4 mm and plastic ties were used to provide a limited horizontal restraint, keeping the side plates in place during the test setup (Figure 6(b)). Figure 6(b) shows extended flange lengths – all the test samples required an extra length of 70 mm at either end to fit the grips of the UTM.

3.1.2 Material properties and connection design

Material coupon tests carried out on the source 6 mm S275JR steel plate according to BS EN ISO 6892-1:2016 (BSI, 2016) established an average yield strength of 283 MPa (±4.7% coefficient of variation) and an average ultimate strength of 476 MPa (±1.8% coefficient of variation) for the material, compared with a minimum yield strength of $f_y = 275$ MPa and a minimum ultimate tensile strength of $f_u = 410$ MPa specified by BS EN 10025-2:2004 (BSI, 2004b). Taking the minimum values for strength as the characteristic values for design, the test and geometry were designed such that the initial yield and failure would occur in the side plates rather than the flange, with yielding expected in the side plates at a load of 42.9 kN.

Table 2 shows the relationships between key design parameters for the scaled flange connection. It was assumed that flexural theory applies to the flange teeth. The simplified plastic design resistance procedure for the connection was carried out in accordance with BS EN 1993-1-1:2005

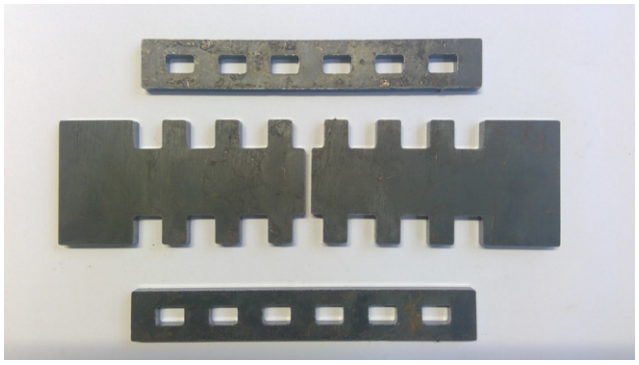

(a)

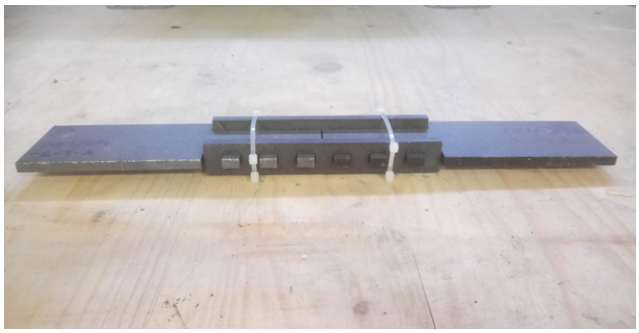

(b)

Figure 6. Flange geometry: (a) example as-fabricated; (b) assembled for testing

(BSI, 2014; Lam *et al.*, 2014) and takes account of axial forces in the flange and the side plates, in addition to combined bending and shear in the flange teeth. Therefore, the number of teeth required on each side of the flange, n_t, depends on the applied axial load on each side of the flange, F_{ti}, and the calculated plastic shear resistance of each flange tooth, $V_{pl,Rd}$, limited to 75%. In this study, a flange tooth width of $b_t = 10$ mm was initially assumed, which allowed calculation of $V_{pl,Rd}$. Assuming an equal distribution of load between the teeth, n_t can be calculated using Equation 1. A simple expression allowing the length of the side plate, l_{sp}, to be calculated is shown in Equation 2. A tolerance $g_0 = 1$ mm was (Table 2); this defines the lateral gap between the side plate and the flange between the teeth. As a result, g_0 is also dependent on the flange tooth corner radius, r_t. Here, $r_t = g_0 = 1$ mm.

Bending deformation of the side plate about its centroidal axis was not considered in the design approach presented here and thus is not considered in Equation 2. Although its effect is presumed to be very small based on flexural testing (Shemshadian *et al.*, 2020), further analysis is needed to quantify the effect of bending deformation on the side plate and hence l_{sp}; this analysis is outside the scope of this paper. The design parameters in Table 2 are reviewed in Section 5 based on the results of experimental testing of the axial behaviour of the connection.

1. $$n_t = \frac{F_{ti}}{0.75\ V_{pl,Rd}}$$

2. $$l_{sp} = 2n_t(b_t + 1) + b_t(2n_t + 1)$$

Following Table 2, the design procedure allowed the resistance of the connection to be calculated and compared for the three component parts at yield – (*a*) the flange section resistance in tension (44.6 kN), (*b*) the flange teeth resistance in shear (57.2 kN) and bending (46.3 kN) and (*c*) the tension resistance of the side plates (42.9 kN). This confirmed that resistance is governed by the side plate capacity and thus yielding should occur in the side plates first.

3.2 Tensile test results and discussion

Figure 7 shows the load–displacement behaviour of the six side ISC flanges tested (samples A–F), obtained from the DIC measurement system. Consistent ductile behaviour across all tests was observed. Differences at the start of the figure at low load and displacements are caused by the initial 'bedding in' or settlement of the connection as teeth come into contact with the side plates. This region only occurred in approximately the first 1.2 mm of displacement, indicating that it was a direct result of the design and fabrication tolerances (1 ± 0.2 mm) and did not significantly affect load-carrying capacity. Figure 8 shows the corresponding load–displacement behaviour with the initial settlements removed, highlighting the consistency between tests. Each sample exhibited some strain-softening behaviour immediately prior to tensile failure, which occurred in the flange rather than the side plates. The failure mechanism is shown in Figure 9 – the failure surface occurred at an incline from corner to corner rather than as a failure surface perpendicular to the direction of loading.

This unexpected failure mechanism was initially investigated by reviewing the load performance of the connection. The average yield load from testing was 46.7 kN while the average ultimate load was 74.8 kN, 1.6 times the yield load. The average yield load exceeded the design value of 42.9 kN. Referring to Section 3.1.2 and Figure 5, this can be partially explained by considering the flange cross-section with an effective area of 162 mm^2; the 46.7 kN yield load corresponds to a stress of 288 MPa, which is closer to the yield strength obtained from material testing (283 MPa) than the value used for design (275 MPa). The ultimate load corresponds to a stress of 462 MPa, clearly higher than the design value but lower than the ultimate strength obtained from material testing. For the side plates, the yield and ultimate loads corresponded to stresses of 299 MPa and 479 MPa, respectively. Although this yield stress exceeded the value obtained from

Table 2. Design data and parameters of scaled side ISC flange connection in S275 steel

	Design value
Flange section properties	
Flange total width: mm	50
Reduced flange width at teeth: mm	27
Flange thickness, t_f: mm	6
Flange effective area, A_f: mm	162
Design plastic axial resistance of flange, $f_y \times A_f$: N	44 550
Side plate properties	
Side plate thickness, t_{sp}: mm	6
Total side plate width provided: mm	20
Side plate hole width: mm	7
Side plate hole length: mm	11
Side plate net effective area, A_{sp}: mm^2	78
Design plastic axial resistance of side plates, $2(f_y A_{sp})/\gamma_{M0}$: N	42 900
Connection properties	
Number of teeth per flange side, n_t	3
Tooth width, b_t: mm	10
Tooth length, l_t: mm	11.5
Tooth shear area, $A_{v,tooth} = t_f \times b_t$: mm^2	60
Tooth plastic section modulus, $W_{pl,z,tooth} = (t_f \times b_t^2)/4$: mm^3	150
Design shear resistance – flange teeth	
Flange force = yield capacity of side plate, F_t: N	42 900
Flange force per side, $F_{ti} = F_t/2$: N	21 450
Design shear force in tooth, $V_{Ed} = F_{ti}/n_t$: N	7150
Shear yield strength, $\tau_y = f_y/\sqrt{3}$: MPa	158.8
Tooth plastic shear resistance, $V_{pl,Rd} = A_{v,tooth}\tau_y/\gamma_{M0}$: N	9526
Design bending resistance – flange teeth	
Bending stress reduction factor, $1-\rho$ ($\rho = [(2V_{Ed}/V_{pl,Rd}) - 1]^2$)	0.749
Reduced yield strength for shear area, $f_{yr} = (1-\rho)\, f_y$: MPa	205.9
Tooth design bending moment, $M_{Ed} = V_{Ed}(t_{sp}/2 + g_0)$: N.mm	28 600
Tooth plastic moment resistance, $M_{pl,Rd} = W_{pl,z,tooth} f_y/\gamma_{M0}$: N.mm	41 250
Reduced tooth plastic moment resistance, $M_{pl,V,Rd} = (1-\rho)M_{pl,Rd}$: N.mm	30 892
Side plate design resistance	
Required side plate effective area, $A_{sp,req} = F_{ti}/f_y$: mm^2	78
Required side plate effective width, $A_{sp,req}/t_{sp}$: mm	13
Total side plate width required: mm	20
Maximum resistances of connection components	
Flange – maximum resistance – axial: N	44 550
Flange teeth – maximum resistance in shear: N	57 158
Flange teeth – maximum resistance in bending: N	46 337
Side plates – maximum axial resistance as per design: N	42 900

material testing, very limited yielding in tension was observed in the side plates, suggesting that this stress concentration did not materialise, potentially due to the load distribution. The flange teeth were observed to deform permanently due to bending in-plane, as shown by the curved edges of the teeth in Figure 9, with the largest deformations in the teeth furthest from the centre of the connection. This also indicates that the teeth at this location potentially carry more load share than the others. Furthermore, due to the load-transfer mechanism, this deformation also caused some slight lateral bending in-plane in the side plates, perpendicular to the direction of loading. This had the effect of increasing the lever arm of moment of the force applied to the end teeth as the ends of the side plates tended to move slightly outwards, away from the flange. Overall, as the same material was used for both the flanges and side plates, the failure shown in Figure 9 is thus most likely caused by the connection geometry as fabricated, or the loading arrangement, or a combination of both.

The failure mechanism was further investigated by inspecting the DIC strain contours obtained during testing (Figure 10). Prior to failure, strains started to increase in the flanges at the point where the cross-section narrows, as expected, although there was an asymmetrical concentration in the top half focused on the right-hand side. Inspecting Figures 10(a)–10(c) in order, the sample can also be seen to shift to the left slightly during testing, which may have caused an imbalance in loading between the two side plates and induced some rotation in the flange, leading to a stress concentration on one side and hence the inclined failure surface between the corners shown in Figure 9. This is investigated further in Section 4.2.2.

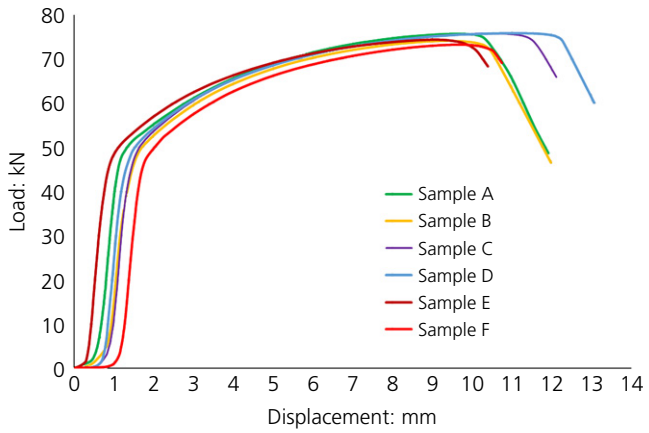

Figure 7. Load–displacement behaviour of scaled side ISC flanges. A full-colour version of this figure can be found on the ICE Virtual Library (www.icevirtuallibrary.com)

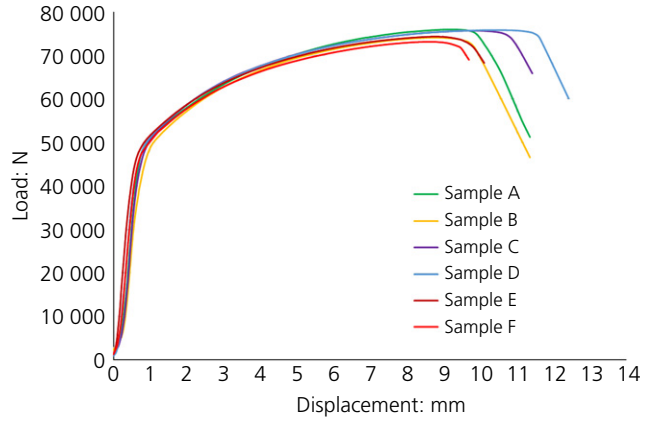

Figure 8. Load–displacement behaviour of scaled side ISC flanges with initial settlement removed. A full-colour version of this figure can be found on the ICE Virtual Library (www.icevirtuallibrary.com)

To prevent the occurrence of this type of failure, the introduction of a larger radius at re-entrant corners (i.e. increasing the width at the base of the flange teeth) may be needed, which could reduce stress concentrations (Schultz *et al.*, 2019; Shemshadian *et al.*, 2020). Overall, the consistency of the behaviour in the scaled testing highlights that it is important to be aware of this in future analysis and design of the full-scale connection, particularly if fabrication and assembly tolerances are relatively large or if a design restricting failure to the side plates is preferred. If the latter is preferred, with the side plates acting as sacrificial elements that can be replaced, a capacity design approach could be used such that the ultimate capacity of the side plates is used to design and detail the flange teeth, although this may result in an overly conservative design with a requirement for significantly more teeth that will

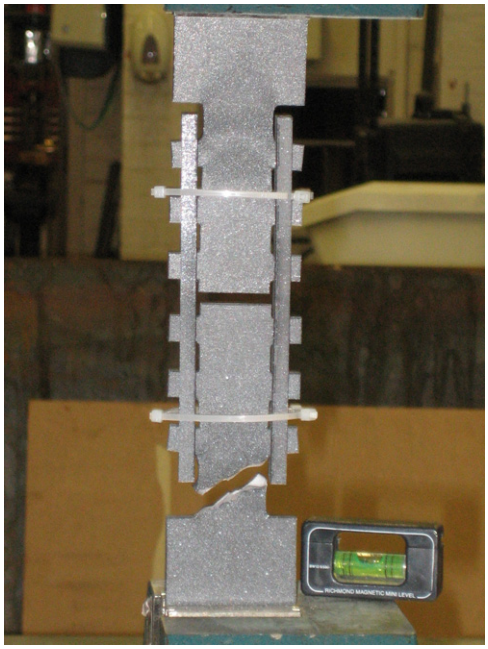

Figure 9. Failure mechanism of scaled side ISC flanges

increase the length of the side plate. Alternatively, a reduction in the effective area of the side plate would be required. To this end, a revision of the design approach presented in Section 3.1.2 is proposed in Section 5.

4. FEA of the axial behaviour of the side ISC

To obtain a more comprehensive understanding of the axial behaviour of the side ISC flange connection observed during testing, non-linear FEA of the experimentally tested connection geometry was undertaken using Abaqus/CAE (DSSC, 2019). As highlighted earlier in the paper, the fabricated geometry and loading arrangement were two influences on the behaviour observed in testing that needed to be considered. Therefore, the effects of fabrication tolerance and lateral movement during testing on the finite-element model (FEM) were also investigated.

4.1 FEM description

For the purposes of the non-linear FEA in Abaqus/Standard, a three-dimensional model of the tested connection geometry was assembled, as shown in Figure 11(a). This model was based on the geometry shown in Figure 5 and is denoted SP1. Geometric and material non-linearity effects were incorporated. All parts were meshed using C3D8R brick elements, as shown in Figures 11(b) and 11(c). A mesh convergence study was carried out that identified 1.5 mm as a suitable element size for mesh refinement, resulting in a total of 25 592 elements and 35 290 nodes for the whole model. The base of the bottom flange was fixed, while the top of the upper flange was restrained in all but the vertical direction to enable

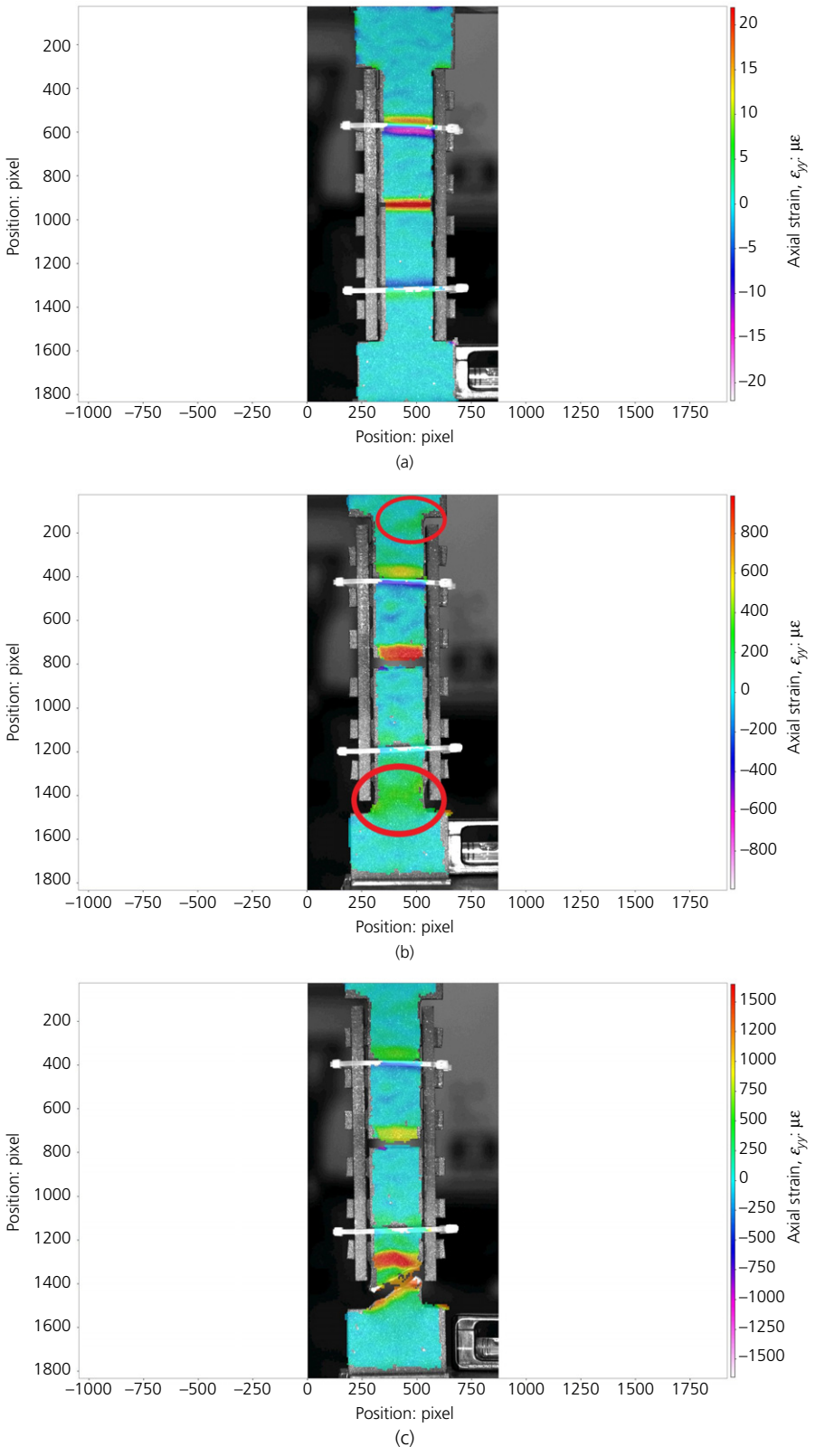

Figure 10. Strain contours from DIC: (a) initial stage; (b) prior to failure; (c) at failure. A full-colour version of this figure can be found on the ICE Virtual Library (www.icevirtuallibrary.com)

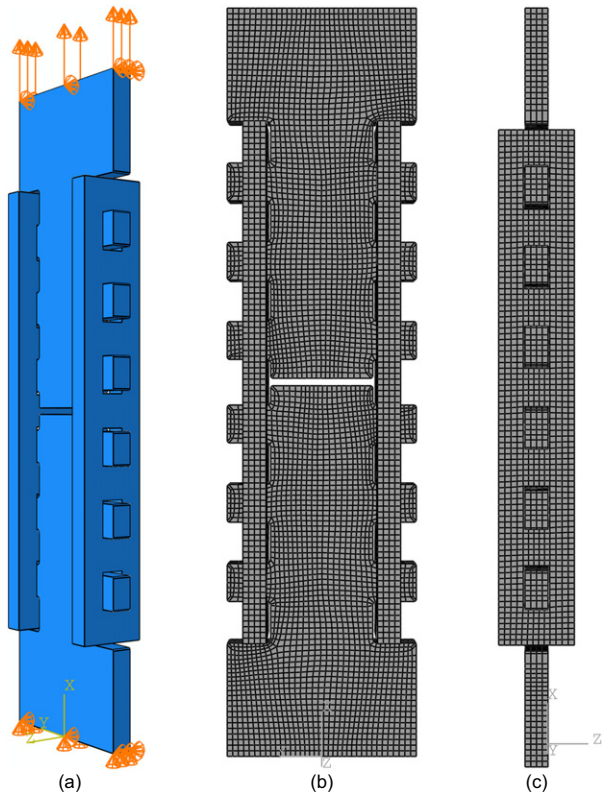

Figure 11. FEM of connection SP1: (a) assembly; (b) mesh front view; (c) mesh end view

a displacement-controlled analysis up to a translation of 14 mm, replicating the experimental test scenario.

4.1.1 Material properties

Two non-linear material models were considered in the analysis. The first was a non-linear, experimentally calibrated, standardised constitutive model for hot-rolled carbon steels (Yun and Gardner, 2017), which can be defined based on only the yield stress f_y, ultimate stress f_u and Young's modulus E of the material. Herein, this model is referred to as the YG model; it was used to represent predicted connection behaviour based on the characteristic design values for S275 steel ($f_y = 275$ MPa, $f_u = 410$ MPa and $E = 210\,000$ MPa). The second material model was based on the experimentally determined stress–strain curve and this was used to investigate the impact of material overstrength on the performance of the connection. The true stress–true strain curves for both material models are shown in Figure 12, with the difference between them clearly illustrating the material overstrength. Poisson's ratio of $v = 0.3$ was adopted for both material models and damage (i.e. fracture) was not incorporated.

4.1.2 Contact interaction between connection surfaces

To model the contact behaviour and transfer of forces between the flange teeth and the side plates, surface-to-surface contact

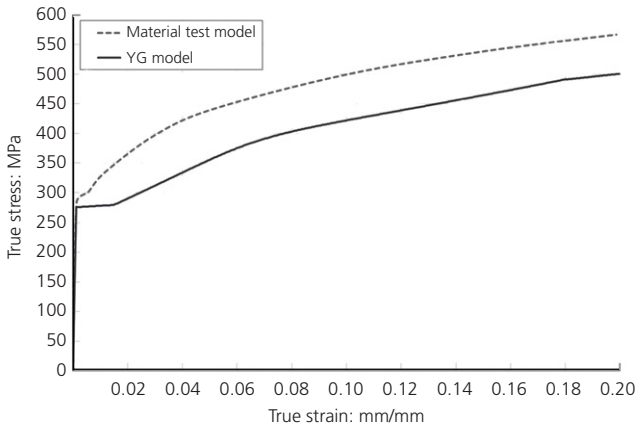

Figure 12. Steel material models adopted for FEA

with finite relative sliding was implemented using the general contact algorithm in Abaqus. It was assumed that all teeth were initially in contact. For the normal contact behaviour, the 'penalty' constraint enforcement method was employed using the default 'hard' contact pressure–overclosure relationship. Tangential behaviour was modelled using the default penalty friction formulation and the isotropic Coulomb friction model. A friction coefficient of 0.3 was selected based on early parametric studies by the authors (Matis *et al.*, 2018a) and also in agreement with the value of 0.3 recommended for bolted connections in international standards (BSI, 2005, 2011).

4.2 FEA results and discussion

The load–displacement responses obtained for each material model from the FEM for SP1 are shown in Figure 13, along with the experimental results for comparison. The general load–displacement behaviour trend was captured well by the FEA. Samples A–F exhibited a slightly lower stiffness in the elastic range during testing, which – combined with the effects

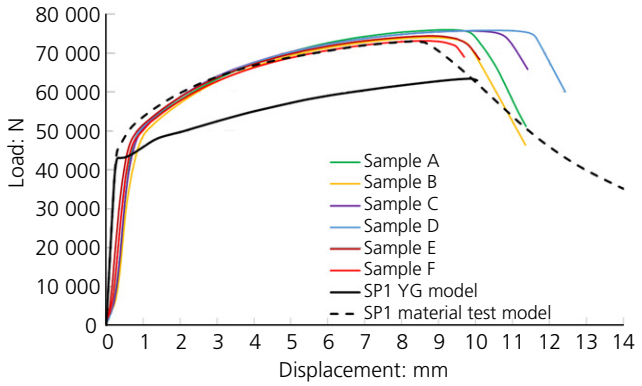

Figure 13. Load–displacement behaviour of FEM SP1 and experimental test samples. A full-colour version of this figure can be found on the ICE Virtual Library (www.icevirtuallibrary.com)

of initial bedding in not being accounted for in the analysis – resulted in yield at a slightly higher displacement and load than in the FEA. However, inspecting the YG model curve, it is clear that the connection outperformed the predicted behaviour based on characteristic design values, verifying a conservative design procedure. The material test model underestimated the average ultimate capacity and corresponding displacement by 2.8% and 9.3%, respectively, but captured the ductile behaviour of the connection very well up to that point, illustrating that the axial behaviour of the connection can be predicted accurately by FEA with material testing. The underestimation highlights that additional capacity is potentially provided by the tested samples that is not explained by material overstrength alone; this is investigated in the next section.

To investigate the unexpected failure location in the flange in testing, the von Mises stress contours at yield strength were inspected. These are shown in Figure 14, with arrows indicating the location of the maximum stresses. Only the contours for the material test model are shown here as the YG model provided similar observations. It can be seen in Figure 14(b) that, aside from the local stress concentrations at the base of the teeth, the teeth furthest from the middle of the connection experienced higher stresses than those the teeth that were closer. It was also found that the yield strength (283 MPa) was first exceeded locally in the flange at the base of the teeth due to the stress concentration, despite the curved corner radius of $r_t = 1$ mm. This is a clear indication of the stress concentration that caused failure in the flange during testing, rather than the side plate, and this relates to tooth bending; this bending can be seen more clearly in Figure 15(a) and agrees well with the experimental observations .

However, the full side plate cross-section yielded first, as per the design, while the ultimate strength (476 MPa) was also exceeded locally in the side plate section first, followed shortly by necking as the full side plate cross-section exceeded the ultimate strength, illustrated by the grey areas in Figure 15(b), which led to complete section failure (i.e. fracture at this location). At this stage, the flange section had fully yielded but only exceeded the ultimate strength locally at the base of the teeth (Figure 15(a)). Irrespective of the failure location, a design revision, including an increased tooth corner radius, may be necessary to reduce the stress concentration in the flange that influenced the failure observed in testing. Note that the influence of the stress concentration is slightly exaggerated at this scale due to the 4 mm extra tooth length on each side of the flange, which reduced the effective flange cross-sectional area by 23%; this extra length would not normally be required at full scale.

4.2.1 Effect of fabrication tolerance on connection behaviour

The laser cutting fabrication tolerance was small for the test samples (±0.2 mm) but, at this scale, could influence the connection capacity. Noting the underestimation of capacities in Figure 13 and the failure location in the flange in testing, the original model was modified to investigate this effect. This modification involved increasing the side plate capacity at the holes, initially according to the specified tolerance of

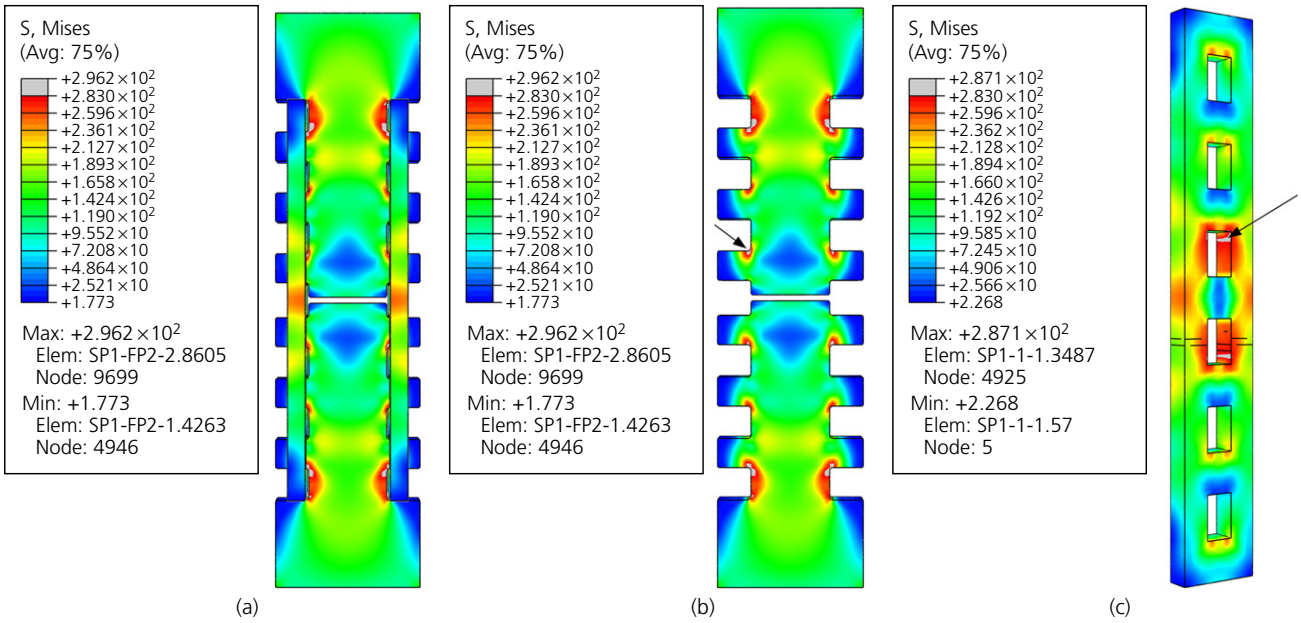

Figure 14. Stress contours for material test FEM SP1 at yield: (a) full model; (b) flanges; (c) side plate (units in MPa). A full-colour version of this figure can be found on the ICE Virtual Library (www.icevirtuallibrary.com)

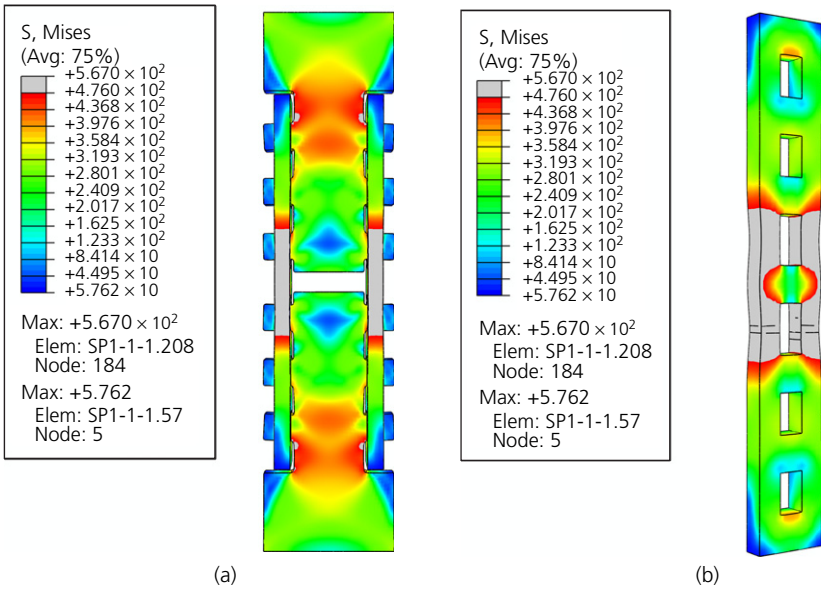

Figure 15. Stress contours for material test FEM SP1 at ultimate connection capacity: (a) full model; (b) side plate (units in MPa). A full-colour version of this figure can be found on the ICE Virtual Library (www.icevirtuallibrary.com)

0.2 mm per edge. However, on inspection of untested samples, the average hole width was found to be 6.3 mm; thus, in the modified model (called SP3), the side plate hole dimensions were reduced to 6.3 mm × 11 mm, from 7 mm × 11 mm. It is important to note that based on the material test model with $f_y = 283$ MPa, this modification increased the axial load capacity of the side plates at yield by 5.4% to 46.5 kN, which was greater than the yield capacity of the flange at 45.9 kN. This is a scenario unique to this test due to the extra 4 mm tooth length either side of the flange.

As shown in Figure 16, the load–displacement curve obtained using the modified model (SP3) provided an excellent match to the experimental results. The average ultimate capacity and corresponding displacement were overestimated by 2.8% and 0.5%, respectively, reflecting some additional capacity that was not present in testing. Based on this figure, it is clear that the fabrication tolerance influenced the behaviour, but the true behaviour lies somewhere between the tolerance used for the SP1 and SP3 models.

The von Mises stress contours at yield are presented in Figure 17. Similar behaviour to Figure 14 for SP1 was observed, with local yield occurring in the flange initially due to the stress concentrations at the base of the teeth, rather than its lower relative yield capacity alone. However, it was found that the ultimate strength was exceeded locally in the flange first for the SP3 model, reflecting the increased side plate capacity. Subsequently, in Figure 18, similar to Figure 15, the ultimate connection capacity was reached when the full side plate cross-section exceeded the ultimate strength and necking

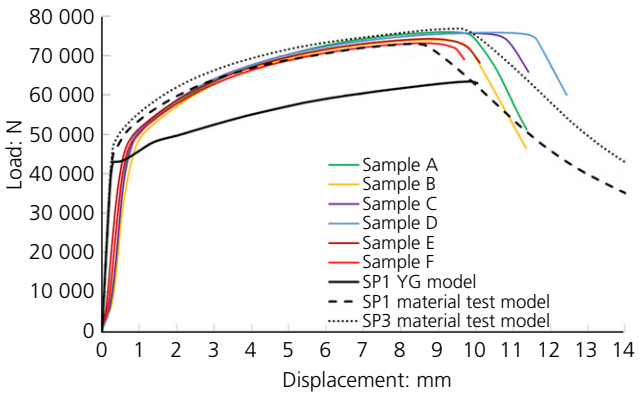

Figure 16. Load–displacement behaviour of FEM SP3 and experimental test samples. A full-colour version of this figure can be found on the ICE Virtual Library (www.icevirtuallibrary.com)

begins. Figure 18 also shows that a much larger area of the flange exceeded the ultimate strength compared with Figure 15, because the side plate could transfer more load; this indicates that fabrication tolerance should be considered as an influence on increased stresses in the flange for the scaled connection design that was tested. At full scale, this influence will become relatively insignificant.

4.2.2 Effect of lateral in-plane displacement

As some lateral movement was observed during testing, a lateral in-plane displacement of up to 6 mm applied at the loaded edge of SP3 was investigated. However, it was found to

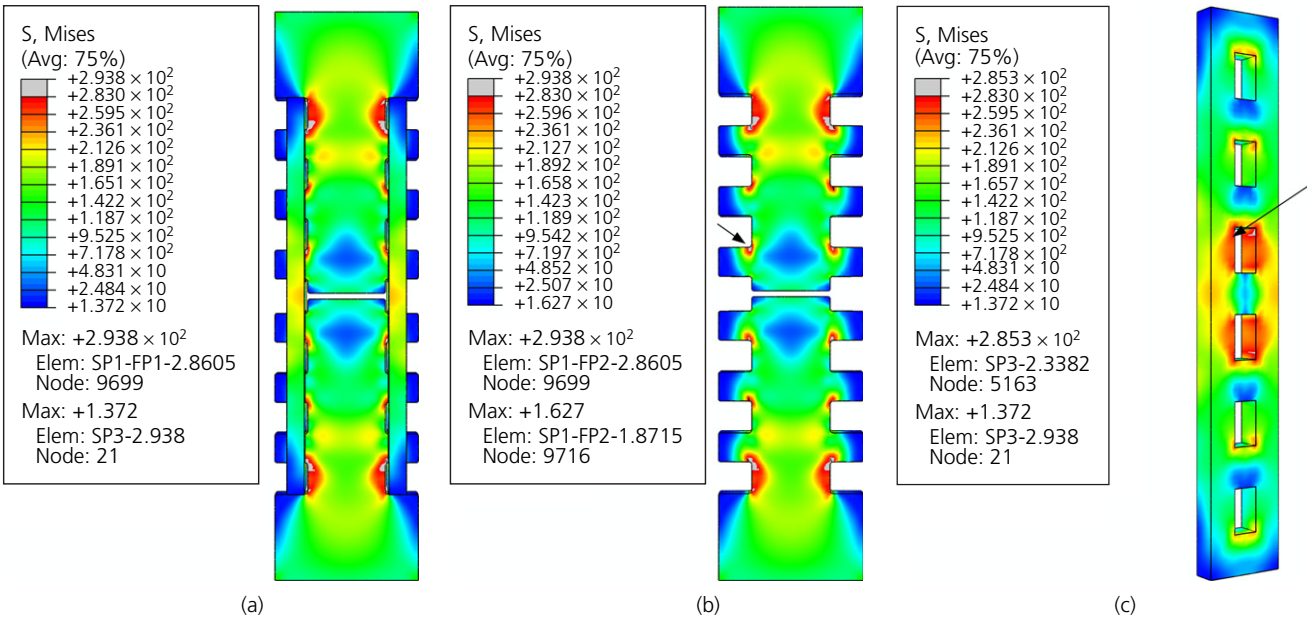

Figure 17. Stress contours of material test FEM SP3 at yield: (a) full model; (b) flanges; (c) side plate (units in MPa). A full-colour version of this figure can be found on the ICE Virtual Library (www.icevirtuallibrary.com)

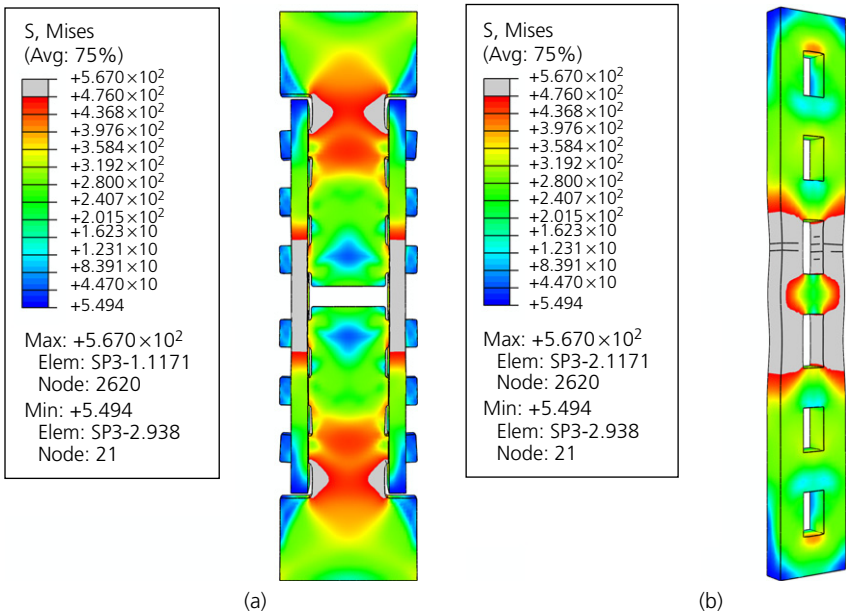

Figure 18. Stress contours for material test FEM SP3 at ultimate capacity: (a) full model; (b) side plate (units in MPa). A full-colour version of this figure can be found on the ICE Virtual Library (www.icevirtuallibrary.com)

have a negligible effect on load–displacement behaviour of the connection, so is not discussed further. In terms of the stress distribution, the trend between the flanges and side plates followed the original SP3 model, with local yield in the flange first followed by full yield of the side plate cross-section and subsequent failure occurring in the side plates. This suggests some further adjustment in the model boundary conditions may be required to fully reflect the local stress concentration causing the fracture observed in the flange in testing. However, an asymmetrical stress distribution can be seen in the flanges in Figure 19, which reflects the stress concentration at the failure location in testing, shown in Figure 10(b). The ultimate

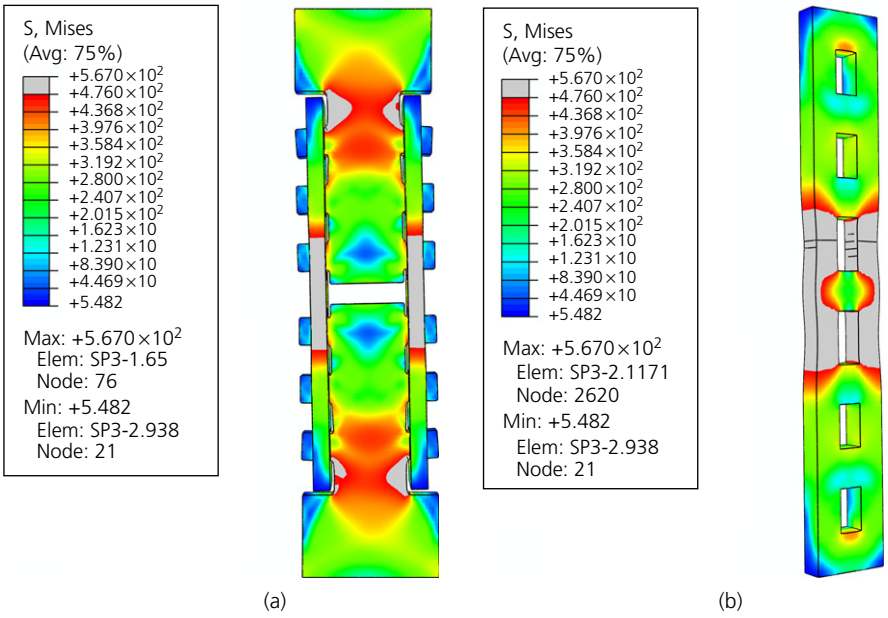

Figure 19. Stress contours for material test SP3 model with lateral displacement at ultimate capacity: (a) full model; (b) side plate (units in MPa). A full-colour version of this figure can be found on the ICE Virtual Library (www.icevirtuallibrary.com)

capacity of the connection corresponded to an in-plane lateral displacement of 3 mm at the loaded edge, in the left-hand direction in Figure 19(a).

5. Review of design and recommendations

Further to the discussion in Section 3.2, based on the observations of the connection behaviour in experimental testing and the non-linear FEA, the design parameters presented in Table 2 and Equation 1 were reviewed. The original design was based on characteristic design strengths, with the side plate at its full yield capacity (42.9 kN) and flange tooth shear and bending utilisation ratios of 75% and 93%, respectively.

Updating this design considering the material yield strength ($f_y = 283$ MPa) and the average yield capacity of the connections ($F_t = 46.7$ kN) obtained from experimental testing, and using the expressions in Table 2, highlights the extent by which the design resistances were exceeded in testing. Firstly, the tooth shear force exceeded the adopted 75% plastic shear resistance limit $(0.75V_{pl,Rd})$ by 4%. Secondly, the tooth bending moment M_{Ed} exceeded the reduced tooth plastic moment resistance $M_{pl,V,Rd}$ by 12%, while the side plate axial load capacity was exceeded by only 6%; this indicates that the flange experienced higher stress concentrations due to tooth bending, as observed in the FEA and reflected by the flange fracture in testing.

Overall, any updated design should

(*a*) guarantee yielding of the full side plate cross-section while the flange section's global behaviour is elastic
(*b*) account for fabrication and construction tolerances
(*c*) account for potential material overstrength influencing side ISC connection behaviour
(*d*) maintain all design resistances within their acceptable limits.

Regarding (*a*) and (*d*), the connection's ultimate capacity should also be controlled by the side plate cross-section reaching the ultimate strength. Considering the original design without the longer flange teeth required for scaled testing (i.e. with l_t revised to 7.5 mm), the axial load capacity of the flange cross-section alone increases by 30% from 44.6 kN to 57.8 kN due to the corresponding increase in cross-sectional area. The results of the FEA for this revision are shown in Figure 20 for the YG design material model; the SP3 side plate was used here to account for fabrication tolerances. It was found that the full side plate cross-section yielded first, as desired, with yielding in the flange restricted to local regions at the base of the teeth corresponding to the stress concentrations observed in the original analyses. The side plate also controlled the ultimate capacity, as desired, with stresses in the flange reaching 402 MPa but not exceeding the ultimate strength at the same localised regions. The FEM of this connection reached an ultimate capacity of 66.7 kN.

5.1 Revision of connection design yield resistances

In addressing item (*b*) of the above list, two cases can be considered for yielding of the side plates based on this study – one each for the maximum and minimum potential yield resistances ($F_{y,sp,max}$ and $F_{y,sp,min}$, respectively). The connection's

nominal design resistance can be based on $F_{y,sp,min}$ as per the original design but the teeth and flange dimensions should be based on $F_{y,sp,max}$, which takes account of potentially increased side plate capacity due to manufacturing tolerances (e.g. the modified design described in Section 4.2.1). Maintaining the same nominal design resistance for the scaled connection

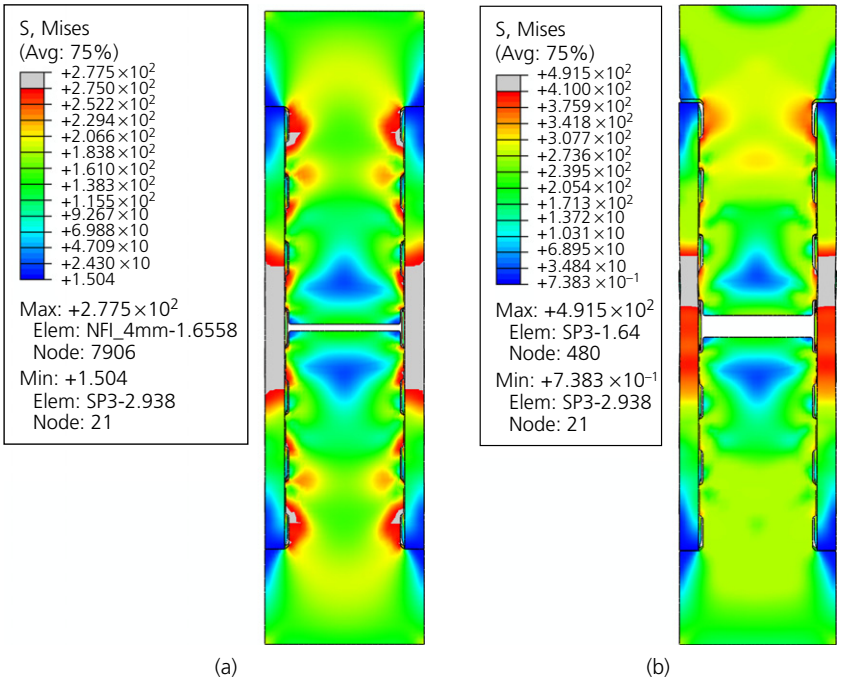

Figure 20. Stress contours for FEM of revised design with $l_t = 7.5$ mm: (a) at yielding of side plate; (b) at ultimate capacity (units in MPa). A full-colour version of this figure can be found on the ICE Virtual Library (www.icevirtuallibrary.com)

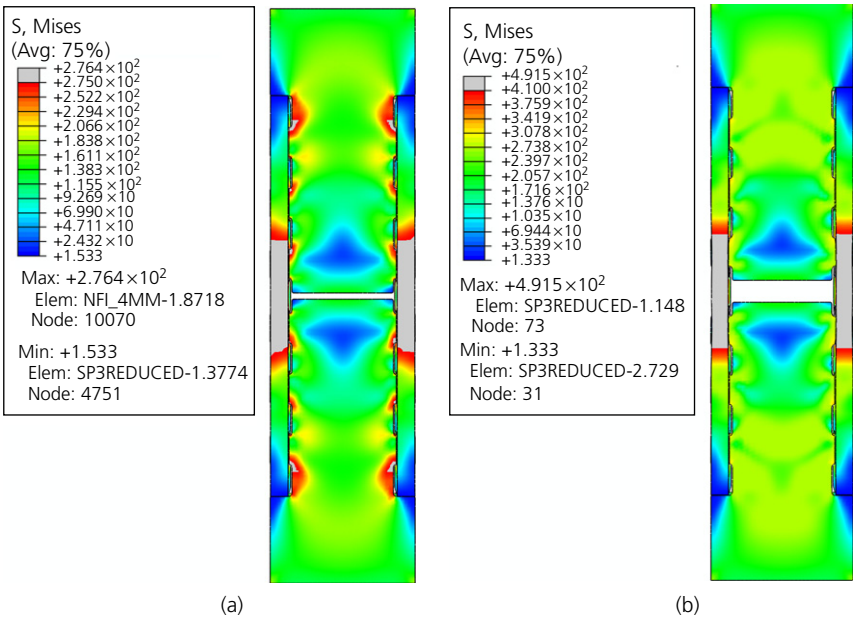

Figure 21. Stress contours for FEM of revised design based on reduced side plate section with $F_{y,sp,min} = 39.6$ kN: (a) at yielding of side plate; (b) at ultimate capacity (units in MPa). A full-colour version of this figure can be found on the ICE Virtual Library (www.icevirtuallibrary.com)

design presented in Section 3.1.2, $F_{y,sp,min} = 42.9\,kN$, which will result in a requirement for the same side plate effective cross-section; however, $F_{y,sp,max} = 45.2\,kN$, which requires an increased flange cross-section. Alternatively, maintaining the original flange cross-section and tooth dimensions, the side plate effective cross-sectional area can be reduced by taking $F_{y,sp,max} = 42.9\,kN$ to provide the desired behaviour. This was achieved by reducing the side plate width from 20 mm to 19 mm, with this reducing the nominal design yield resistance of the connection to $F_{y,sp,min} = 39.6\,kN$ – a reduction of 7.7%. This reduction was applied to the SP3 FEM for analysis of the design solution. The resulting stress contours at yielding of the side plate cross-section and ultimate connection capacity are presented in Figure 21, which shows the desired behaviour. The FEM for this connection reached an ultimate capacity of 61.8 kN, reflecting the reduced side plate cross-section capacity. Local stress concentrations in the flange were again observed to occur, but the maximum stress in the flange never exceeded 339 MPa.

5.2 Effect of increasing the number of flange teeth

Additional factors can be introduced to promote the desired connection yield and failure behaviour, which also address points (*a*)–(*d*) listed earlier in Section 5, such as increasing the width or the number of flange teeth, which will reduce the influence of stress concentrations at the base of the teeth. For this purpose, an alternative recommendation based on this study is to use Equation 3 with the expressions in Table 2 to calculate a revised number of flange teeth required for a beam section using characteristic design values. Using the scaled geometry tested as part of this study as an example, with the same side plate cross-section and assuming no change in flange tooth dimensions, $n_{t,rev} = 4$ rather than the $n_t = 3$ used in the original design. This straightforward revision increases the length of the side plates

Table 3. Maximum design resistances of connection components for revised design parameters

	Design revision			
Component	$l_t = 7.5$ mm	$n_{t,rev} = 4$	Updated $F_{y,sp,max}$ and $F_{y,sp,min}$	$b_t = 11$ mm; $r_t = 2.6$ mm
Flange – axial resistance: N	57 750	57 750	57 750	52 470
Flange teeth – shear resistance: N	57 158	76 210	57 158	62 873
Flange teeth – bending resistance: N	46 337	81 194	46 337	46 367
Side plates – axial resistance, $F_{y,sp,min}$: N	42 900	42 900	39 600	39 600
Stress concentration factor for flange from FEA	2.7	2.1	2.6	2.5

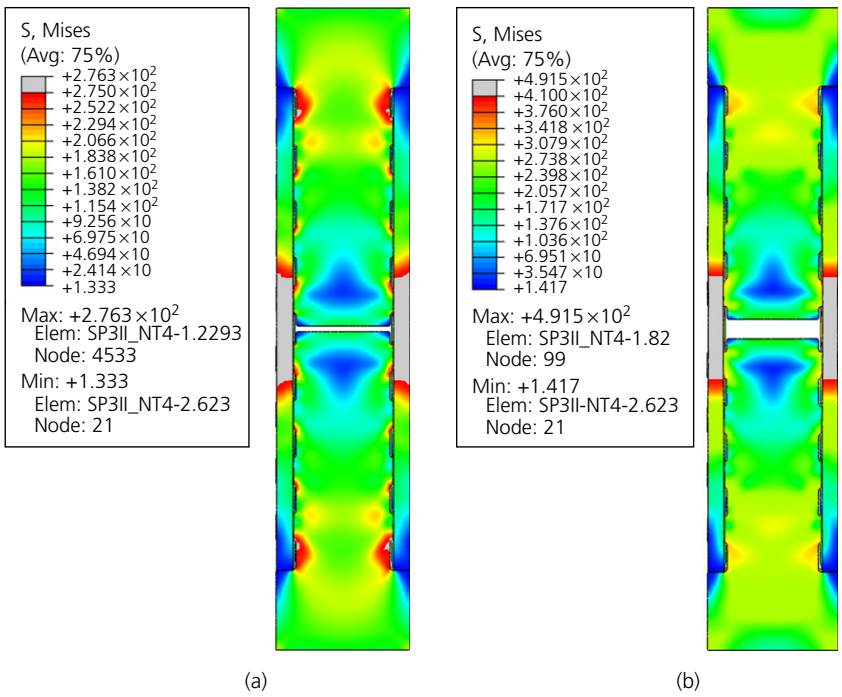

Figure 22. Stress contours for FEM of revised design with $n_{t,rev} = 4$: (a) at yielding of side plate; (b) at ultimate capacity (units in MPa). A full-colour version of this figure can be found on the ICE Virtual Library (www.icevirtuallibrary.com)

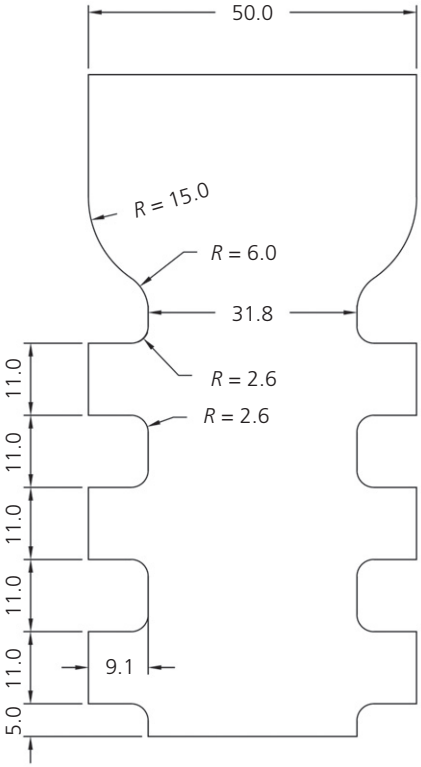

Figure 23. Revised flange geometry investigated for scaled side ISC

but reduces the individual flange tooth shear and bending utilisation ratios to 56% and 53%, respectively, and was found to reduce the associated stress concentrations observed in this study. It can be seen in Table 3 that the flange stress concentration factor reduces from 2.7 to 2.1, a reduction of 20%. Hence, this solution has residual capacity, which allows for material overstrength. The associated von Mises stress contours at both full yield of the side plate cross-sections and ultimate connection capacity are shown in Figure 22. Again, the desired behaviour was achieved, with the connection yield and ultimate capacities controlled by the side plate. Similar to the design with $l_t = 7.5$ mm, an ultimate capacity of 66.7 kN was achieved in the FEA. Also, the maximum stress reached locally in the flange was 361 MPa, well below the ultimate strength.

3. $$n_{t,rev} = \frac{F_{ti}}{0.75\ V_{pl,Rd}} + 1$$

5.3 Effect of varying the flange tooth width and corner radius

In Section 4.2, it was proposed to increase the flange tooth corner radius r_t to reduce the stress concentration in the flange. However, any increase in this radius is equivalent to both a reduction in the flange width (i.e. axial resistance) and an increase in g_0 (i.e. the lever arm increases by the same amount for the resultant force of the side plate applied to the flange tooth). Therefore, for the original design presented

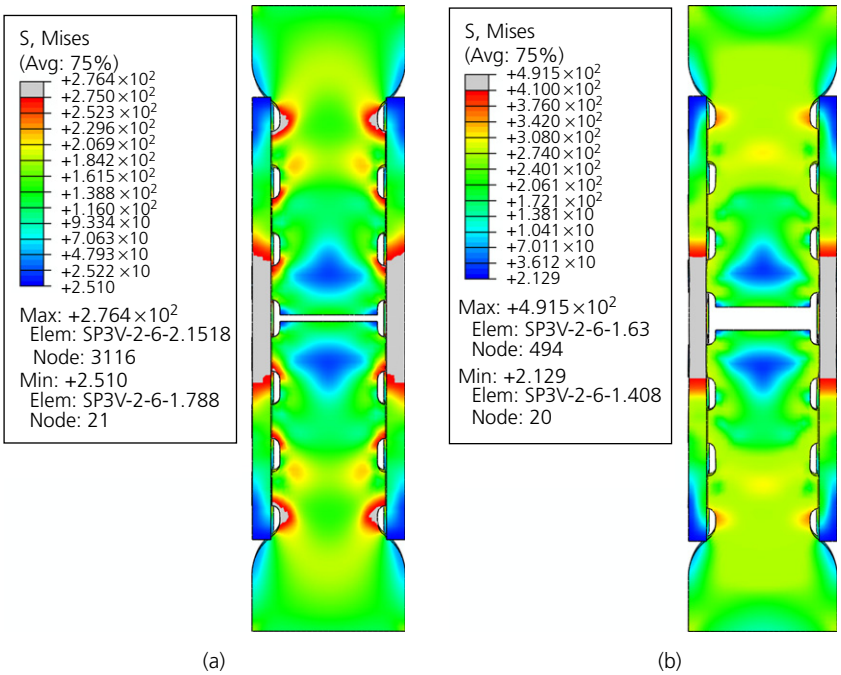

Figure 24. Stress contours for FEM of revised design with $b_t = 11$ mm and $r_t = 2.6$ mm: (a) at yielding of side plate; (b) at ultimate capacity (units in MPa). A full-colour version of this figure can be found on the ICE Virtual Library (www.icevirtuallibrary.com)

in this paper, the radius cannot exceed $r_t = 1.3$ mm without reducing the design capacity of the flange. This can be partially addressed by increasing the flange tooth width b_t. To investigate this, a limited parametric study was carried out based on the expressions in Table 2 to identify a pair of values of b_t and r_t that can maintain the original bending capacity of the flange teeth at 46.3 kN without reducing the flange axial capacity below that of the side plates. This resulted in values of $b_t = 11$ mm and $r_t = 2.6$ mm, as shown in Figure 23, with the resulting stress contours for this FEM shown in Figure 24. Again, the desired behaviour was achieved, although the flange stress concentration factor was only reduced from 2.7 (for the reduced l_t model) to 2.5 in this case. The ultimate connection capacity observed from the FEA was 61.9 kN while the maximum stress reached locally in the flange was 382 MPa. Further increases to the corner radius are not possible without a reduction in the capacity of the flange cross-section, thus the use of extra teeth as per Equation 3 may be preferrable to achieve higher resistances and lower stress concentrations for the same flange section width.

Further increases in the tooth width b_t would also increase tooth bending and shear resistances but also cause the length of the side plate to increase, potentially influencing bending deformation of the side plate, which is not currently considered in the design. Future work will need to analyse this behaviour in greater detail to establish its significance for the flexural behaviour of the connection at full scale.

Table 3 provides a summary of the design resistances for all of the above design revisions. The calculated values given for the side plate are based on the design geometry (i.e. SP1 type side plate), while the SP3 type with higher resistance was used in the FEA to account for fabrication tolerance.

6. Conclusions

This paper has outlined the work carried out in a collaborative tripartite project between the USA, Republic of Ireland and Northern Ireland to create and investigate the design, development and testing of a new class of ISCs that rely on neither welding nor bolting, targeting the facilitation of fast disassembly of steel structures and material reuse. This connection type could potentially offer a time saving of 62.5% over conventional bolted connections. The front ISC was introduced with a summary of a numerical study of its behaviour under mixed-mode loading scenarios, highlighting its excellent shear resistance and noting its limitations in terms of axial and flexural capacity with respect to erection tolerances.

These limitations motivated the development of the side ISC, for which the results of scaled experimental testing and non-linear FEA of the axial behaviour of the flange connection have been presented here. The connection exhibited ductile behaviour, and the measured yield and ultimate load capacities were in close agreement with experimentally determined material properties, highlighting the extent of material over-strength over the characteristic values used in design. An unexpected but consistent tensile failure pattern was observed in the flange rather than in the side plates where it was expected; this was influenced by a combination of the material over-strength, the loading arrangement during testing and the fabrication tolerance of the sample geometry, leading to an asymmetrical stress distribution, as confirmed by FEA. This has implications for future design and testing of this connection type at full scale, particularly if side plates are to be designed to fail by yielding first or if fabrication and assembly tolerances are relatively large. As a result, the calculations of the connection design resistance were revised in the design procedure, supported by FEA of the effect of varying geometric parameters including the flange tooth radius and length and the number of flange teeth required. Increasing the number of flange teeth was found to reduce the flange stress concentrations while maintaining the connection capacity.

Work is ongoing in the AMASS project, with upcoming full-scale experimental testing of the behaviour and performance of the side ISC in a structural frame. This is expected to support the establishment of a straightforward design method to enable adoption by designers in industry.

Acknowledgements

The research presented in this paper is part of a collaboration and partnership between Queen's University Belfast, University College Dublin and the University of Minnesota. The authors wish to express their gratitude for the funding received from the US–Ireland Research and Development Partnership Programme, supported by the Department for Education (DfE) and Invest Northern Ireland (grant USI-096), the National Science Foundation (grant CMMI-1563115), Science Foundation Ireland (grant SFI/15/US/B3234) and Enterprise Ireland (grant CF20160454).

REFERENCES

Adan SM and Gibb W (2008) Inelastic cyclic testing of the Kaiser bolted bracket moment connection. *Proceedings of Structures Congress 2008: Crossing Borders, Vancouver, BC, Canada* (Anderson D, Ventura C, Harvey D and Hoit M (eds)). American Society of Civil Engineers, Reston, VA, USA, pp. 1–10.

Adan SM and Gibb W (2009) Experimental evaluation of Kaiser bolted bracket steel moment-resisting connections. *Engineering Journal* **46(3)**: 181–195.

AISC (American Institute of Steel Construction) (2016a) ANSI/AISC 358-16: Prequalified connections for special and intermediate steel moment frames for seismic applications. AISC, Chicago, IL, USA.

AISC (2016b) ANSI/AISC 360-16: Specification for structural steel buildings. AISC, Chicago, IL, USA.

Al-Sabah A and Laefer D (2017a) GB Patent Application 1718744.4, Nov.

Al-Sabah A and Laefer D (2017b) GB Patent Application 1718746.9, Nov.

Al-Sabah AS, Laefer DF, Truong-Hong L *et al.* (2020) Introduction of the intermeshed steel connection—a new universal steel connection. *Buildings* **10(3)**: 37, https://doi.org/10.3390/buildings10030037.

BCSA (British Constructional Steelwork Association), Steel for Life and SCI (The Steel Construction Institute) (2018a) *Recycling and Reuse*. See https://www.steelconstruction.info/Recycling_and_reuse (accessed 08/01/2019).

BCSA, Steel for Life and SCI (2018b) *Simple Connections*. See https://www.steelconstruction.info/Simple_connections (accessed 11/06/2018).

BSI (2004a) ISO 7500-1: Metallic materials. Verification of static uniaxial testing machines. Tension/compression testing machines. Verification and calibration of the force-measuring system. BSI, London, UK.

BSI (2004b) BS EN 10025-2:2004: Hot rolled products of structural steels. Technical delivery conditions for non-alloy structural steels. BSI, London, UK.

BSI (2005) BS EN 1993-1-82005: Eurocode 3. Design of steel structures. Design of joints. BSI, London, UK.

BSI (2011) BS EN 1090-2:2008+A1:2011: Execution of steel structures and aluminium structures – part 2: technical requirements for steel structures. BSI, London, UK.

BSI (2014) BS EN 1993-1-1:2005+A1:2014: Eurocode 3. Design of steel structures. General rules and rules for buildings. BSI, London, UK.

BSI (2016) BS EN ISO 6892-1:2016: Metallic materials. Tensile testing. Method of test at room temperature. BSI, London, UK.

Burgan B (2002) *Report to DTI: Pilot Application of a new Steelwork Connection*, 1st edn. The Steel Construction Institute, Ascot, UK.

ConXtech (2020) See https://www.conxtech.com (accessed 20/10/2020).

Cordova PP and Hamburger RO (2011) Steel connections: Proprietary or public domain? *Modern Steel Construction* **51(10)**: 24–31.

DSSC (Dassault Systèmes Simulia Corp.) (2019) *ABAQUS documentation*. DSSC, Providence, RI, USA.

Engelhardt MD, Winneberger T, Zekany AJ and Potyraj T (1998) Experimental investigation of dogbone moment connections. *Engineering Journal* **35(4)**: 128–139.

FEMA (Federal Emergency Management Agency) (2000) FEMA-350: Recommended seismic design criteria for new steel moment-frame buildings. FEMA, Washington, DC, USA.

Fleischman RB, Viscomi BV and Lu LW (1990) *ATLSS Connections – Concept, Development and Experimental Investigation*. ATLSS report number 91-02. See http://preserve.lehigh.edu/engr-civil-environmental-atlss-reports/165 (accessed 21/10/2020).

GVR (Grand View Research) (2019) *Structural Steel Market Size, Share & Trends Analysis Report By Application, By Region, And Segment Forecasts, 2019–2025*. GVR, San Francisco, CA, USA, Report ID: 978-1-68038-503-8. See https://www.grandviewresearch.com/industry-analysis/structural-steel-market (accessed 21/10/2020).

Hamburger RO (2006) Prequalified connections for special and intermediate steel moment frames for seismic applications, ANSI/AISC 358-05. In *Proceedings of Structural Congress 2006* (Cross B and Finke J (eds)). American Society of Civil Engineers, Reston, VA, USA pp. 1–8. See https://doi.org/10.1061/40889(201)5 (accessed 20/10/2020).

Hamburger RO, Krawinkler H, Malley J and Adan S (2009) *NEHRP Seismic Design Technical Brief No. 2: Seismic Design of Steel Special Moment Frames: A Guide for Practicing Engineers*. NIST, Gaithersburg, MD, USA.

Han SW and Moon KH (2007) Cyclic behaviour of post-Northridge WUF-b connections. *Journal of Constructional Steel Research* **63(3)**: 365–374, https://doi.org/10.1016/j.jcsr.2006.05.003.

Heywood MD (2004) *Quicon Design Guide to BS 5950-1*. The Steel Construction Institute, Ascot, UK.

Jin J and El-Tawil S (2005) Seismic performance of steel frames with reduced beam section connections. *Journal of Constructional Steel Research* **61(4)**: 453–471.

Krar S and Gill A (2003) *Exploring Advanced Manufacturing Technologies*. Industrial Press Inc., New York, NY, USA.

Lam D, Ang T and Chiew SP (2014) *Structural Steelwork – Design to Limit State Theory*. CRC Press, Boca Raton, FL, USA.

LaVision (2018) *StrainMaster Systems*. See http://www.lavision.de/en/products/strainmaster/systems/index.php (accessed 03/09/2019).

Lindapter (2018) See http://www.lindapter.com/About/History (accessed 01/06/2018).

Matis P, Martin T, McGetrick PJ and Robinson D (2018a) The effect of frictional contact properties on intermeshed steel connections. In *Proceedings of the Civil Engineering Research in Ireland Conference, CERI2018* (Pakrashi V and Keenahan J (eds)). Civil Engineering Research Association of Ireland, Dublin, Ireland, Paper 199, pp. 547–553,

Matis P, Martin T, McGetrick PJ and Robinson D (2018b) Modelling and experimental testing of interlocking steel connection behaviour. *Proceedings of the 6th International Symposium on Life-Cycle Civil Engineering, IALCCE 2018, Ghent, Belgium* (Caspeele R, Taerwe L and Frangopol DM (eds)). CRC Press/Balkema, London, UK, Paper 666.

Muller C and Oppe M (2008) Conceptual design and design examples for multi-storey buildings. Eurocodes: background and applications. EN 1993 Eurocode 3: design of steel structures. *Dissemination of Information for Training Workshop, Brussels, Belgium*. See https://eurocodes.jrc.ec.europa.eu/doc/WS2008/EN1993_6_Mueller.pdf (accessed 26/06/2018).

Naimi S, Celikag M and Hedayat AA (2013) Ductility enhancement of post-Northridge connections by multi-longitudinal voids in the beam web. *Scientific World Journal* **2013**: 515936, https://doi.org/10.1155/2013/515936.

NSAI (National Standards Authority of Ireland) (2018) IS EN ISO 12944-3:2017. Paints and varnishes – Corrosion protection of steel structures by protective paint systems – Part 3: Design considerations. NSAI, Dublin, Ireland.

Perreira ND, Fleischman RB, Viscomi BV and Lu LW (1993) *Automated Construction and ATLSS Connections; Development, Analysis, Experimentation, and Implementation of ATLSS Connections for Automated Construction*. ATLSS report number 93-02. See https://preserve.lehigh.edu/engr-civil-environmental-atlss-reports/183 (accessed 26/06/2018).

Rafezy B, Huynh Q, Gallart H and Kheirollahi M (2015) An innovative method for the seismic retrofitting of existing steel moment frame structures using side plate technology. *Proceedings of the 2nd ATC & SEI Conference on Improving the Seismic Performance of Existing Building and Other Structures, San Francisco, CA, USA*, pp. 144–158.

Rafezy B, Huynh Q and Adams J (2018) Numerical and experimental analysis of an innovative steel special moment frame connection. *Proceedings of the 11th National Conference on Earthquake Engineering 2018 (11NCEE): Integrating Science, Engineering, & Policy, Los Angeles, CA, USA*. Earthquake Engineering Research Institute (EERI) and Curran Associates, Inc., pp. 763–766.

Ramakrishnan S and Rogozinski MW (1997) Properties of electric arc plasma for metal cutting. *Journal of Physics D: Applied Physics* **30(4)**: 636–644.

SAC JV (SAC Joint Venture) (1995) *Interim Guidelines: Evaluation, Repair, Modification and Design of Steel Moment Frames*. SAC JV, Sacramento, CA, USA, Report no. SAC-95-02.

Sansom M and Avery N (2014) Reuse and recycling rates of UK steel demolition arisings. *Proceedings of the Institution of Civil*

Engineers – Engineering Sustainability **167(3)**: 89–93, https://doi.org/10.1680/ensu.13.00026.

Schultz A, Le JL, Shemshadian M *et al.* (2019) AMASS: Advanced Manufacturing and Assembly of Steel Structures. *Proceedings of the 10th International Structural Engineering and Construction Conference (ISEC-10), Chicago, IL, USA* (Ozevin D, Ataei H, Modares M, *et al.* (eds)). ISEC Press, Fargo, ND, USA, Paper STR-80.

Shemshadian ME, Le JL, Schultz AE *et al.* (2019) Numerical study of the behavior of intermeshed steel connections under mixed-mode loading. *Journal of Constructional Steel Research* **160**: 89–100. See https://doi.org/10.1016/j.jcsr.2019.04.024.

Shemshadian ME, Labbane R, Schultz AE *et al.* (2020) Experimental study of intermeshed steel connections manufactured using advanced cutting techniques. *Journal of Constructional Steel Research* **172**: 106169. See https://doi.org/10.1016/j.jcsr.2020.106169.

SRI (Steel Recycling Institute) (2017) *Steel is the World's Most Recycled Material*. SRI, Southfield, MI, USA, See https://www.steelsustainability.org/recycling (accessed 07/01/2019).

Stojadinovic B, Goel SC and Lee KH (2000) Development of post-Northridge steel moment connections. *Proceedings of the 12th World Conference on Earthquake Engineering, 12WCEE, Auckland, New Zealand*. New Zealand Society for Earthquake Engineering, Upper Hutt, New Zealand, vol. 1269.

Sutton MA, Orteu JJ and Schreier H (2009) *Image Correlation for Shape, Motion and Deformation Measurements: Basic Concepts, Theory and Applications*. Springer, Boston, MA, USA. See https://doi.org/10.1007/978-0-387-78747-3.

UMG (Urban Modeling Group) (2019) *Intermeshed Steel Connection: Frame Erection Test*. See https://www.youtube.com/watch?v=zRWl5qpAjNc (accessed 03/09/2019).

Yun X and Gardner L (2017) Stress-strain curves for hot-rolled steels. *Journal of Constructional Steel Research* **133**: 36–46. See https://doi.org/10.1016/j.jcsr.2017.01.024.

How can you contribute?

To discuss this paper, please email up to 500 words to the editor at journals@ice.org.uk. Your contribution will be forwarded to the author(s) for a reply and, if considered appropriate by the editorial board, it will be published as discussion in a future issue of the journal.

Proceedings journals rely entirely on contributions from the civil engineering profession (and allied disciplines). Information about how to submit your paper online is available at www.icevirtuallibrary.com/page/authors, where you will also find detailed author guidelines.